

COMPARATIVE PLANETARY ATMOSPHERES: MODELS OF TRES-1 AND HD209458B

J. J. FORTNEY¹, M. S. MARLEY¹, K. LODDERS², D. SAUMON³, R. FREEDMAN^{1,4}*Accepted to ApJ Letters, May 17, 2005*

ABSTRACT

We present new self-consistent atmosphere models for transiting planets TrES-1 and HD209458b. The planets were recently observed with the *Spitzer Space Telescope* in bands centered on 4.5 and 8.0 μm , for TrES-1, and 24 μm , for HD209458b. We find that standard solar metallicity models fit the observations for HD209458b. For TrES-1, which has an $T_{\text{eff}} \sim 300$ K cooler, we find that models with a metallicity 3-5 times enhanced over solar abundances can match the 1σ error bar at 4.5 μm and 2σ at 8.0 μm . Models with solar abundances that included energy deposition into the stratosphere give fluxes that fall within the 2σ error bars in both bands. The best-fit models for both planets assume that reradiation of absorbed stellar flux occurs over the entire planet. For all models of both planets we predict planet/star flux ratios in other *Spitzer* bandpasses.

Subject headings: planetary systems, radiative transfer, binaries:eclipsing, stars: individual (TrES-1), stars: individual (HD209458)

1. INTRODUCTION

The detection of photons emitted by an extrasolar planet is a landmark feat in the history of astronomy. Ten years after the initial discovery of the first extrasolar giant planet (EGP) 51 Peg b (Mayor & Queloz 1995), Charbonneau et al. (2005) report a detection of infrared flux from TrES-1 and Deming et al. (2005b) report a similar detection for HD209458b. Both observations were made with the *Spitzer Space Telescope* as each planet passed behind its parent star. While a number of papers have aimed at predicting the optical and infrared spectra of hot EGPs (Seager & Sasselov 1998; Marley et al. 1999; Barman et al. 2001; Sudarsky et al. 2003), these results are the first infrared detections (rather than upper limits) that can be compared with models.

TrES-1, discovered by Alonso et al. (2004), is similar to the well-known planet HD209458b (Charbonneau et al. 2000; Henry et al. 2000) in mass and orbital period but it receives less stellar irradiation and has a significantly smaller radius. Sozzetti et al. (2004) and Laughlin et al. (2005) have recently placed tighter constraints on the planet's mass and radius by improving our knowledge of the physical parameters of the parent star.

TrES-1 and HD209458b are members of the class of "Pegasi planets" (or "hot Jupiters") that orbit their parent stars at less than ~ 0.1 AU and are presumed to be tidally locked. Unlike brown dwarfs of similar effective temperature, the luminosity of Pegasi planets is dominated by absorbed and re-radiated stellar flux, rather than intrinsic luminosity due to cooling of its interior. Atmospheric dynamics will redistribute this absorbed energy around the planet with an efficiency that is currently unknown (Showman & Guillot 2002; Cho et al. 2003; Burkert et al. 2005; Cooper & Showman 2005). Because of the dominance of absorbed flux over intrinsic flux, the planet's effective tem-

perature T_{eff} , is equal to its equilibrium temperature, T_{eq} , given by:

$$T_{\text{eq}}^4 = f(1 - A)L_{\star}/(16\pi\sigma d^2), \quad (1)$$

where f is 1 if the absorbed radiation is able to be radiated away over the entire planet (4π steradians) or 2 if it only radiates on the day side (2π steradians). A is the planet's Bond albedo, L_{\star} is the luminosity of the star, σ is the Stefan-Boltzmann constant, and d is the planet's orbital distance.

2. REVIEW OF THE OBSERVATIONS

Charbonneau et al. (2005) used the Infrared Array Camera (IRAC) aboard *Spitzer* to observe the emission of the combined TrES-1 planet/star system. The timing of the observations included time before, during, and after the secondary eclipse (when the planet's light is blocked by the star). The observations were performed simultaneously in bands 2 and 4, centered on 4.5 and 8.0 μm , respectively. The planet+star system was indeed brighter in both bands when the planet was visible, indicating thermal emission from the planet was detected. The observed eclipse depths, in units of relative flux, were 0.00066 ± 0.00013 at 4.5 μm and 0.00225 ± 0.00036 at 8.0 μm . The HD209458b observations by Deming et al. (2005b) utilized this same method, except that their observation used the Multiband Imaging Photometer for *Spitzer* (MIPS) instrument at 24 μm . The observed flux ratio was 0.00260 ± 0.00046 .

From their observations Charbonneau et al. (2005) derived brightness temperatures in each of the two bands, $T_{4.5} = 1010 \pm 60$ K and $T_{8.0} = 1230 \pm 110$ K. It is important to notice that $T_{8.0} > T_{4.5}$, which was not predicted by models of Pegasi planets cited above, nor for brown dwarfs of similar T_{eff} (Marley et al. 1996; Burrows et al. 1997; Al-

¹ NASA Ames Research Center, Space Science and Astrobiology Division, MS 245-3, Moffett Field, CA 94035; jfortney@arc.nasa.gov, Mark.S.Marley@nasa.gov, freedman@darkstar.arc.nasa.gov

² Planetary Chemistry Laboratory, Department of Earth and Planetary Sciences, Washington University, St. Louis, MO 63130; lodders@levee.wustl.edu

³ Los Alamos National Laboratory, MS F699, Los Alamos, NM 87545; dsaumon@lanl.gov

⁴ SETI Institute, 515 N. Whisman Road, Mountain View, CA 94043

lard et al. 2001; Saumon et al. 2003a), nor is it observed in the mid infrared spectra of brown dwarfs to date (Roellig et al. 2004; Patten et al. 2004). Charbonneau et al. (2005) also derive a planetary $T_{\text{eff}} = 1060 \pm 50$ K and $A = 0.31 \pm 0.14$, but as the planet is not a blackbody, the values found are only suggestive. For HD209458b, Deming et al. (2005b) determine a brightness temperature $T_{24} = 1130 \pm 150$ K.

3. METHODS

To obtain our atmospheric pressure-temperature (P - T) profiles and spectra for the planets we employ a 1D model atmosphere code that has been used for a variety of planetary and substellar objects. The code was first used to generate profiles and spectra for Titan by McKay et al. (1989). It was significantly revised to model the atmospheres of brown dwarfs (Marley et al. 1996; Burrows et al. 1997; Marley et al. 2002), Uranus (Marley & McKay 1999), and EGPs (Marley 1998). It explicitly includes both incident radiation from the parent star and thermal radiation from the planet’s atmosphere. The basic radiative transfer solving scheme was developed by Toon et al. (1989). We use the elemental abundance data of Lodders (2003) and compute chemical equilibrium compositions following Fegley & Lodders (1994) and Lodders & Fegley (2002). In addition we maintain a large and constantly updated opacity database. We predict all cloud properties using the model of Ackerman & Marley (2001) with a sedimentation efficiency parameter $f_{\text{sed}} = 3$, which fits spectral observations of cloudy L-dwarfs (Marley et al. 2002). This model places 90% of the optical depth of a cloud within 1 scale height of the cloud base. Further details can be found in Marley et al. (2002) and Marley et al. (in prep).

We model the impinging stellar flux from 0.26 to 10.0 μm and the emitted thermal flux from 0.26 to 325 μm . All the relevant planetary parameters for TrES-1 are taken from Sozzetti et al. (2004). Those for HD209458b are taken from Brown et al. (2001). For the TrES-1 stellar model we use the Kurucz K0V model atmosphere computed for the Charbonneau et al. (2005) paper. For HD209458b we use a Kurucz (1993) G0V model ($L_{\star} = 1.6L_{\odot}$) with parameters described in Brown et al. (2001). The planet’s radiative-convective P - T profile is arrived at iteratively until the net flux is conserved to at least one part in 10^6 . We compute all band-averaged flux density ratios using Eq. (1) from Charbonneau et al. (2005). Our model atmosphere code computes the P - T profile and low resolution spectra covering our full wavelength range. To generate a high-resolution spectrum we take the generated P - T profile and use a full line-by-line radiative transfer code, using the same chemistry and opacity database used in determining the P - T profile and low-resolution spectrum (Saumon et al. 2000).

4. RESULTS

4.1. Atmospheric Pressure-Temperature Profiles

Our computed atmosphere profiles are shown in Figure 1. Two cloudless profiles for TrES-1 are shown, one under the assumption that absorbed stellar radiation is reradiated from the entire planet, and one for the assumption that the planet can only reradiate this energy on the day side. For these cases we derive a T_{eff} of 1134

K and 1352 K, respectively. Both of these profiles assume solar metallicity and an intrinsic temperature, T_{int} of 250 K. This T_{int} is the T_{eff} the planet would have if it were in isolation. For the 4π case we also plot a profile for $T_{\text{int}} = 100$ K, which leads to a deeper radiative zone, but has no effect on the emitted spectrum. The presence of an outer radiative zone is predicted for the atmospheres of all Pegasi planets and is caused by the dominance of external (stellar) radiation over internal heat flux (Guillot et al. 1996). The planet’s current T_{int} can only be derived from thermal evolution models of the planet, which we do not compute here. For the 4π TrES-1 profile we show the model’s range of brightness temperatures in 4.5 and 8.0 μm bands.

We also plot our derived P - T profile for HD209458b. This profile assumes 4π reradiation, solar metallicity, and $T_{\text{int}} = 250$ K. For HD209458b we find $T_{\text{eff}} = 1442$ K, ~ 300 K hotter than that for TrES-1. The model’s brightness temperature at 24 μm is shown as a plus on this profile. We also plot the boundary where CO and CH₄ have the same abundance. We predict CO will be the dominant (but not exclusive) carrier of carbon for both planets. Also shown are the condensation curves for Na₂S, enstatite (MgSiO₃), forsterite (Mg₂SiO₄) and iron (Fe). Clouds form deep in the atmosphere of TrES-1 and therefore have no effect on the planet’s spectrum. For HD209458b, we find that a potential enstatite cloud layer does affect the P - T profile and spectrum, as shown by the dash-dot profile. High clouds in the atmosphere of HD209458b are compatible with the available data from atmospheric transmission spectroscopy (Charbonneau et al. 2002; Fortney et al. 2003; Deming et al. 2005a), although the clouds in those studies are at mbar pressures. Our profile for HD209458b is very similar to the 4π model of Iro et al. (2004), although our profiles show hints of stratospheric temperature inversions due to absorption by near infrared water bands, which to our knowledge other authors have not found.

4.2. Flux Ratios and Brightness Temperatures

Our computed flux ratios for the HD209458b model atmospheres match the Deming et al. (2005b) observation well. We find $\Delta F = 0.00305$ for a cloudless model or with clouds of iron and forsterite, which is within the 1σ error bar. If the silicate cloud is not forsterite, but enstatite, which forms higher in the atmosphere, we find $\Delta F = 0.00316$. Models computed assuming 2π reradiation would be brighter at 24 μm , leading to a poorer fit to the datum.

For TrES-1 we will examine our model atmospheres in detail. In Figure 2 we show three panels of results. Panel A shows the surface flux of the model K0V stellar spectrum along with two computed surface fluxes of planet TrES-1. These spectra are for 2π and 4π reradiation and solar metallicity. As expected, the 2π spectrum is brighter. Note that between 4-10 μm we find that emitted planetary flux is ~ 7 -9 orders of magnitude brighter than reflected stellar flux.

The lower two panels of Figure 2 show the planet/star flux ratio, as would be seen by a distant observer, which folds in the factor of ~ 60 difference in surface area of the planet and star. These panels compare our computed ratios to those measured by Charbonneau et al. (2005).

For 2π reradiation our ratio at $4.5\ \mu\text{m}$ is 4.5σ too high, indicating the planet model is far too luminous at these wavelengths. However, the fit at $8.0\ \mu\text{m}$ is quite good. For the 4π model, the flux at $4.5\ \mu\text{m}$ is a reasonable fit, falling just above 1σ error bars, while at $8.0\ \mu\text{m}$ the model falls below the 2σ error bar. Both of these models have approximately the same infrared spectral slope, which is obviously not as steep as Charbonneau et al. (2005) observed. This slope is mainly controlled by H_2O absorption on the blue side of the $4.5\ \mu\text{m}$ band and strong CO absorption on the red side. At $8.0\ \mu\text{m}$, H_2O and CH_4 are the dominant absorbers. Based on these results, we rule out the 2π model and examine the sensitivity of the spectral slope to model parameters. Our computed brightness temperatures for the 4π models are $T_{4.5} = 1075\ \text{K}$ and $T_{8.0} = 995\ \text{K}$, while Charbonneau et al. (2005) found $T_{8.0} > T_{4.5}$. Compared to a blackbody, the planet is redder while the models are bluer.

A flux deficit at $4.5\ \mu\text{m}$, relative to atmosphere models using equilibrium chemistry, is a common feature of Jupiter and T dwarfs (Golimowski et al. 2004). This is likely due to dredging of CO from deeper layers, which absorbs flux from $4.5\text{-}5\ \mu\text{m}$ (Fegley & Lodders 1996; Saumon et al. 2003b). We find this process cannot affect the atmosphere of TrES-1 as CO is already the dominant carbon-bearing molecule in the planet’s atmosphere.

We also varied the metallicity of the planet’s atmosphere. We computed chemistry and opacity grids at metallicities of 3.2 ($[\text{M}/\text{H}]=0.5$) and 5.0 ($[\text{M}/\text{H}]=0.7$) times solar. Recall that Jupiter’s atmosphere is enhanced in heavy elements by factors of $\sim 2\text{-}4$. With $3.2\times$ or $5\times$ solar metallicity the models fall within the 1σ error bar at $4.5\ \mu\text{m}$ and 2σ at $8.0\ \mu\text{m}$. Panel C of Figure 2 shows the flux ratios for the $5\times$ solar abundance model. Increasing the metallicity by $3.2\times$ decreases the CH_4/CO ratio by an order of magnitude. (The position of $\text{CH}_4/\text{CO}=1$ curve varies inversely proportional to the metal/hydrogen ratio.) This in turn increases the $8.0\ \mu\text{m}$ band flux by weakening the strong CH_4 band at $7.8\ \mu\text{m}$. Increasing the metallicity also increases the amount of H_2O , which decreases the flux on the blue side of the $4.5\ \mu\text{m}$ band.

We also considered whether we could further improve the fit by increasing the C/O ratio from 0.5 (solar) to 0.7 , therefore increasing CO absorption at $4.5\ \mu\text{m}$ and decreasing H_2O absorption at $8.0\ \mu\text{m}$. However, increasing the C/O ratio (by increasing the carbon abundance) *increases* the CH_4 abundance relative to CO (and H_2O) and flux actually decreases in the $8.0\ \mu\text{m}$ band. Increasing $[\text{M}/\text{H}]$ from 0 to $+0.5$ or increasing the C/O ratio from 0.5 to 0.7 has very little effect on the strength of the CO band. This is because the band is formed very high in the atmosphere and is already saturated at solar abundances.

Another avenue we pursued was increasing the temperature of the upper atmosphere. In our models the pressures at which optical depth unity occurs in the $8.0\ \mu\text{m}$ band are slightly smaller than those in the $4.5\ \mu\text{m}$ band, although there is considerable overlap. (See Figure 1.) Therefore, increasing the temperatures at lower pressures preferentially increases the $T_{8.0}$ relative to $T_{4.5}$. We deposited additional energy in the form of a Chapman function (e.g. Chamberlain & Hunten 1987), into the upper atmosphere at pressures ranging from 1 to $10\ \text{mbar}$. Possible unmod-

eled energy sources include conduction downward from a hot thermosphere (Yelle 2004), the breaking of gravity waves, or an unmodeled optical absorber, such as photochemical products. Profiles that warm the atmosphere at $10\ \text{mbar}$ by $\sim 200\ \text{K}$ (requiring $\sim 10^7\ \text{erg cm}^{-2}\ \text{sec}^{-1}$, or 2.5% of the incoming stellar flux) generate more flux in the $8.0\ \mu\text{m}$ band, and reach the 2σ error bars in both bands. Representative flux ratios of one of these models is shown in Panel C of Figure 2.

In another trial (not shown) we modeled a strong continuum opacity source from $2\text{-}6\ \mu\text{m}$. An appropriately strong absorber cuts down the flux in the $4.5\ \mu\text{m}$ band while increasing flux in the $8.0\ \mu\text{m}$ band, which allows the model to fit the 1σ error bars in both bands. It is unclear what this mystery opacity source could be. Liang et al. (2004) found that HD209458b should be free of hydrocarbon hazes as atmospheric temperatures are too high for hydrocarbons to condense. Their conclusion should hold for TrES-1, although it is $\sim 300\ \text{K}$ cooler. We note that the photochemical destruction of CH_4 (Liang et al. 2003) would lead to slightly weaker absorption at $8.0\ \mu\text{m}$.

5. DISCUSSION

We find that a solar metallicity atmosphere for TrES-1 marginally fits the *Spitzer* observations. Models with enhanced metallicity are promising as they fall within the 1σ error bar in the $4.5\ \mu\text{m}$ band and 2σ error bar in the $8.0\ \mu\text{m}$ band. Solar metallicity models with extra energy deposition into the stratosphere fit at the 2σ level. As Table 1 shows, observations with IRAC at $3.6\ \mu\text{m}$ look most promising for further separating the predictions of standard solar abundance models from others. For the model phase space we explore it is extremely difficult to obtain brightness temperatures of $T_{8.0} > T_{4.5}$. One possible remedy would be for the planet to have a cooler troposphere than we predict here, but a much hotter stratosphere, which could cause the planet’s absorption features to become emission features, and vice versa. We can recover this behavior with an ad-hoc $P\text{-}T$ profile. We note that in Jupiter the $7.8\ \mu\text{m}$ CH_4 feature is seen in emission, not absorption.

As shown above, standard solar abundance models fit the Deming et al. (2005b) MIPS observation well. However, with this one data point *metal enhanced atmospheres are not excluded*. The known differences between HD209458b and TrES-1 are the former’s larger radius and higher T_{eff} . It is not yet clear if these atmospheres are substantially different in character. Possibilities include opacity due to silicate condensates in HD209458b but not TrES-1, and opacity due to photochemical products in TrES-1 but not HD209458b. *Spitzer* observations in additional bandpasses for both planets will help to characterize these atmospheres. Observations of the depth of the primary eclipse with *Spitzer* will allow the measurements of nightside fluxes of the planet, which would place strong constraints on atmospheric dynamics and on the energy redistribution between the day/night hemispheres. In Table 1 we collect our computed planet/star flux ratios for a variety of TrES-1 and HD209458b models in all four IRAC bands and the MIPS $24\ \mu\text{m}$ band.

Since models of the mid infrared spectra of brown dwarfs match observations to date (Roellig et al. 2004; Patten

et al. 2004), we suggest that while atmospheric composition plays a role, a complete explanation for the red spectral slope of TrES-1 likely will involve energy from the parent star. Whether this is due to unknown photochemical processes, unmodeled energy sources that dramatically modify the P - T profile, or some other process is not yet clear.

We thank Kevin Zahnle, Joe Harrington, David Charbonneau, and Sara Seager for comments. We acknowledge support from an NRC postdoctoral fellowship (JJF), NASA grants NAG2-6007 and NAG5-8919 (MSM), and NSF grant AST-0406963 (KL). This work was supported in part by the US Department of Energy under contract W-7405-ENG-36.

REFERENCES

- Ackerman, A. S. & Marley, M. S. 2001, *ApJ*, 556, 872
 Allard, F., Hauschildt, P. H., Alexander, D. R., Tamanai, A., & Schweitzer, A. 2001, *ApJ*, 556, 357
 Alonso, R., et al. 2004, *ApJ*, 613, L153
 Barman, T. S., Hauschildt, P. H., & Allard, F. 2001, *ApJ*, 556, 885
 Brown, T. M., Charbonneau, D., Gilliland, R. L., Noyes, R. W., & Burrows, A. 2001, *ApJ*, 552, 699
 Burkert, A., Lin, D. N. C., Bodenheimer, P. H., Jones, C. A., & Yorke, H. W. 2005, *ApJ*, 618, 512
 Burrows, A., et al. 1997, *ApJ*, 491, 856
 Chamberlain, J. W. & Huntent, D. M. 1987, Orlando FL Academic Press Inc International Geophysics Series, 36
 Charbonneau, D., et al. 2005, *ApJ* in press, ArXiv Astrophysics e-prints 0503457
 Charbonneau, D., Brown, T. M., Latham, D. W., & Mayor, M. 2000, *ApJ*, 529, L45
 Charbonneau, D., Brown, T. M., Noyes, R. W., & Gilliland, R. L. 2002, *ApJ*, 568, 377
 Cho, J. Y.-K., Menou, K., Hansen, B. M. S., & Seager, S. 2003, *ApJ*, 587, L117
 Cooper, C. S. & Showman, A. P. 2005, Submitted to *ApJ*, ArXiv Astrophysics e-prints 0502476
 Deming, D., Brown, T. M., Charbonneau, D., Harrington, J., & Richardson, L. J. 2005a, *ApJ*, 622, 1149
 Deming, D., Seager, S., Richardson, L. J., & Harrington, J. 2005b, *Nature*, 434, 740
 Fegley, B. J. & Lodders, K. 1994, *Icarus*, 110, 117
 —. 1996, *ApJ*, 472, L37
 Fortney, J. J., Sudarsky, D., Hubeny, I., Cooper, C. S., Hubbard, W. B., Burrows, A., & Lunine, J. I. 2003, *ApJ*, 589, 615
 Gollimowski, D. A., et al. 2004, *AJ*, 127, 3516
 Guillot, T., Burrows, A., Hubbard, W. B., Lunine, J. I., & Saumon, D. 1996, *ApJ*, 459, L35
 Henry, G. W., Marcy, G. W., Butler, R. P., & Vogt, S. S. 2000, *ApJ*, 529, L41
 Iro, N., Bezdard, B., & Guillot, T. 2004, ArXiv Astrophysics e-prints, 0409468
 Kurucz, R. 1993, ATLAS9 Stellar Atmosphere Programs and 2 km/s grid. Kurucz CD-ROM No. 13. Cambridge, Mass.: Smithsonian Astrophysical Observatory, 1993., 13
 Laughlin, G., et al. 2005, *ApJ*, 621, 1072
 Liang, M., Parkinson, C. D., Lee, A. Y.-T., Yung, Y. L., & Seager, S. 2003, *ApJ*, 596, L247
 Liang, M., Seager, S., Parkinson, C. D., Lee, A. Y.-T., & Yung, Y. L. 2004, *ApJ*, 605, L61
 Lodders, K. 2003, *ApJ*, 591, 1220
 Lodders, K. & Fegley, B. 2002, *Icarus*, 155, 393
 Marley, M. S. 1998, in *Astronomical Society of the Pacific Conference Series*, ed. R. Rebolo, E. L. Martin, M. R. Zapatero Osorio, 383
 Marley, M. S., Gelino, C., Stephens, D., Lunine, J. I., & Freedman, R. 1999, *ApJ*, 513, 879
 Marley, M. S. & McKay, C. P. 1999, *Icarus*, 138, 268
 Marley, M. S., Saumon, D., Guillot, T., Freedman, R. S., Hubbard, W. B., Burrows, A., & Lunine, J. I. 1996, *Science*, 272, 1919
 Marley, M. S., Seager, S., Saumon, D., Lodders, K., Ackerman, A. S., Freedman, R. S., & Fan, X. 2002, *ApJ*, 568, 335
 Mayor, M. & Queloz, D. 1995, *Nature*, 378, 355
 McKay, C. P., Pollack, J. B., & Courtin, R. 1989, *Icarus*, 80, 23
 Patten, B. M., et al. 2004, American Astronomical Society Meeting Abstracts, 205,
 Roellig, T. L., et al. 2004, *ApJS*, 154, 418
 Saumon, D., et al. 2000, *ApJ*, 541, 374
 Saumon, D., Marley, M. S., & Lodders, K. 2003a, ArXiv Astrophysics e-prints, 0310805
 Saumon, D., Marley, M. S., Lodders, K., & Freedman, R. S. 2003b, in *IAU Symposium 211*, ed. E. Martin, 345
 Seager, S. & Sasselov, D. D. 1998, *ApJ*, 502, L157
 Showman, A. P. & Guillot, T. 2002, *A&A*, 385, 166
 Sozzetti, A., et al. 2004, *ApJ*, 616, L167
 Sudarsky, D., Burrows, A., & Hubeny, I. 2003, *ApJ*, 588, 1121
 Toon, O. B., McKay, C. P., Ackerman, T. P., & Santhanam, K. 1989, *J. Geophys. Res.*, 94, 16287
 Yelle, R. V. 2004, *Icarus*, 170, 167

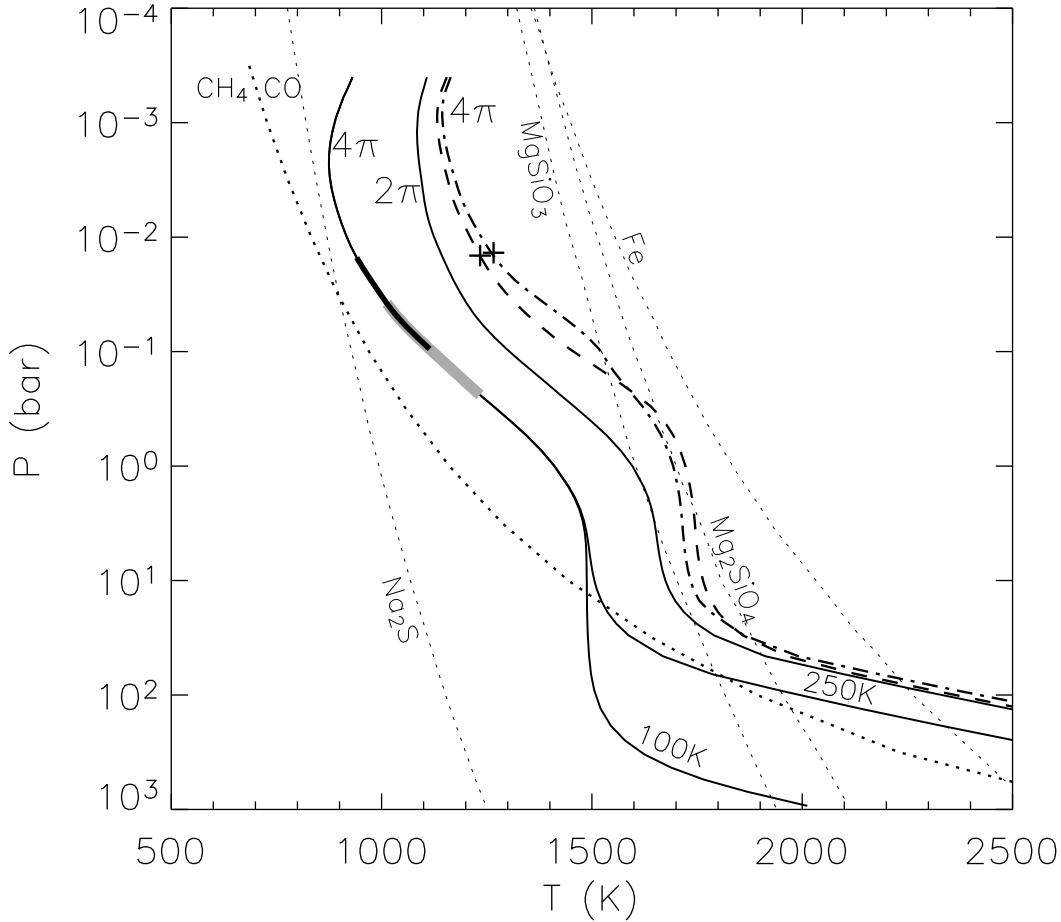


FIG. 1.— Pressure-temperature (P - T) profiles for TrES-1 and HD209458b. The solid lines are two profiles for TrES-1 assuming either 2π (hotter) or 4π (cooler) reradiation of absorbed stellar flux. Both profiles assume $T_{\text{int}} = 250$ K. For the 4π case, we also plot a profile with $T_{\text{int}} = 100$ K. For the 4π profile the thick black portion of the profile shows the extent of the brightness temperatures in the $8.0 \mu\text{m}$ band. The even thicker gray portion of the profile shows the brightness temperatures in the $4.5 \mu\text{m}$ band. We plot two 4π profiles for HD209458b. The dashed line is cloud-free and the dash-dot line includes the opacity of MgSiO_3 and Fe clouds. The model brightness temperatures at $24 \mu\text{m}$ are marked with pluses. The thick dotted line is the boundary where CO and CH_4 have the same abundance. Condensation curves for Na_2S , MgSiO_3 , Mg_2SiO_4 , and Fe are thin dotted lines.

TABLE 1
MODEL FLUX DENSITY RATIOS IN SPITZER BANDS FOR TRES-1 AND HD209458B

Planet	Model	T_{eff}	$3.6 \mu\text{m}$	$4.5 \mu\text{m}$	$5.8 \mu\text{m}$	$8.0 \mu\text{m}$	$24 \mu\text{m}$
TrES-1	4π	1134	0.46	0.81	1.11	1.48	2.93
TrES-1	2π	1352	1.06	1.30	1.69	2.24	3.69
TrES-1	$4\pi, 3.2 \times \text{solar}$	1144	0.58	0.78	1.15	1.62	3.02
TrES-1	$4\pi, 5 \times \text{solar}$	1148	0.61	0.78	1.17	1.66	3.06
TrES-1	$4\pi, \text{heating}$	1165	0.56	0.90	1.24	1.71	3.19
HD209458b	4π	1442	0.96	1.12	1.45	1.90	3.05
HD209458b	$4\pi, \text{cloudy}$	1448	1.02	1.22	1.56	2.01	3.16

Note. — All ratios have been multiplied by 1000. Abundances are solar, unless noted. HD209458b “cloudy” includes enstatite and iron clouds.

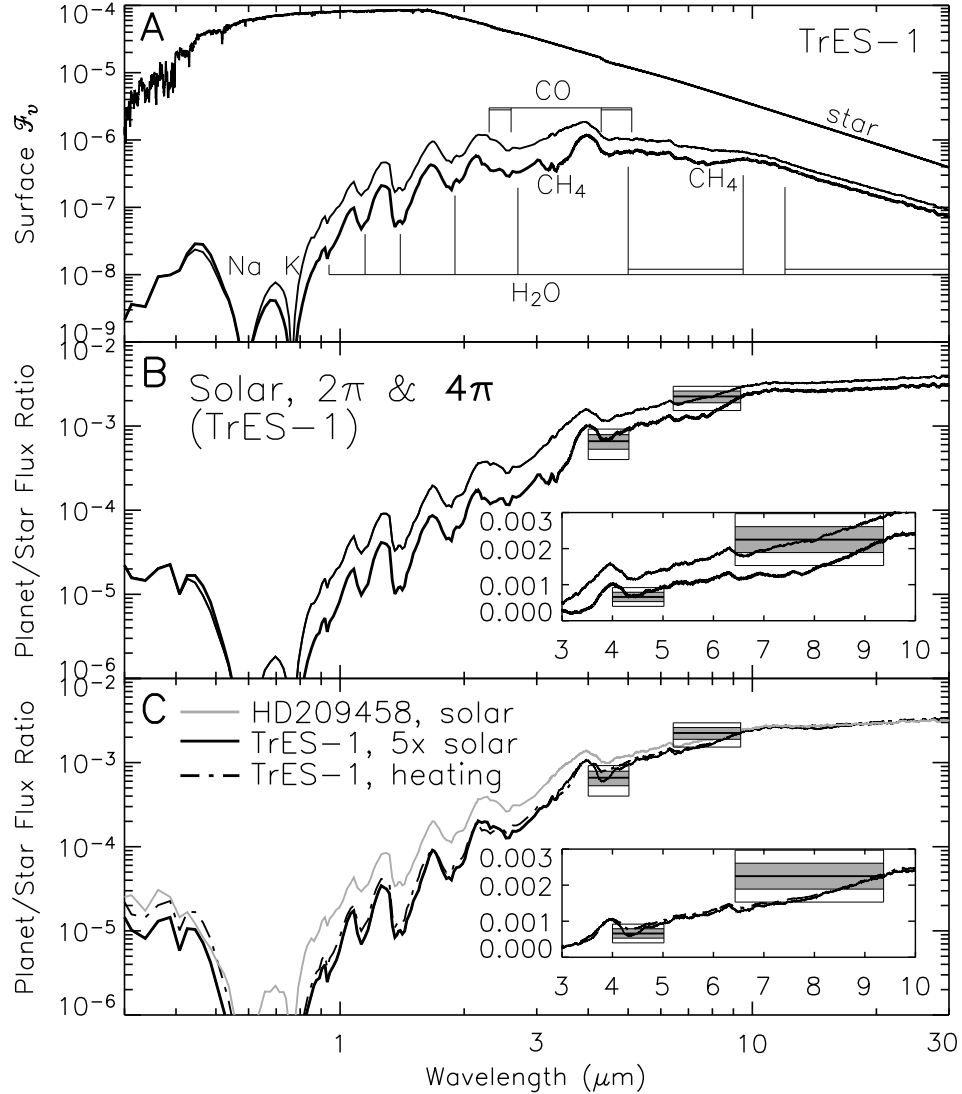


FIG. 2.— Panel A: Emergent surface flux density (in $\text{erg s}^{-1} \text{cm}^{-2} \text{Hz}^{-1}$) for the TrES-1 K0V parent star and two planet models—the higher curve assumes 2π flux reradiation and the lower thick curve 4π . Relevant absorption features are labeled. Panel B: Planet/star flux density ratios for the models in panel A, as viewed by a distant observer. The full-width at half-maximum wavelength range of both bands are shown. The one- and two- σ error bars of the Charbonneau et al. (2005) measurements are shown as shaded boxes and empty boxes, respectively. The inset is a blowup of the 3-10 μm region. Panel C: The gray curve is HD209458, the solid black curve is TrES-1 with 5 times solar metallicity, and the dash-dot curve is TrES-1 with solar metallicity and a heated upper atmosphere. (See text.)